Reconstruction methods for combined HAADF-STEM and EDS tomography

Zhong, Z.

Cover Page

The following handle holds various files of this Leiden University dissertation:
http://hdl.handle.net/1887/67129

Author: Zhong, Z.
Title: Reconstruction methods for combined HAADF-STEM and EDS tomography
Issue Date: 2018-12-10

1

Introduction and outline

The PhD research that is collected in this thesis is dedicated to the development of novel tomographic reconstruction methods for characterizing both structural and compositional information of nanomaterials. In this chapter, first an introduction is given to the two imaging modalities in electron tomography that are central to this thesis: high angle annular dark field scanning transmission electron microscopy (HAADF-STEM) and energy dispersive X-ray spectroscopy (EDS). Second, we formulate the mathematics for the problem of tomographic reconstruction. Finally, we discuss the challenges for performing accurate tomographic reconstructions for individual chemical elements based on these modalities, and give an overview for several methods developed during the PhD research.

1.1 Electron microscopy and tomography

An electron microscope (EM) uses accelerated electrons instead of visible light to image materials at the nanoscale. Conventional EM is based on the same principle as optical microscopy, but with an electron source and electromagnetic lenses. As illustrated in Figure 1.1, a parallel electron beam is formed and used to illuminate the sample. An image is then formed and projected on the camera. This conventional imaging mode is called transmission electron microscopy (TEM). At present, the highest resolution realized in high-resolution TEM is around 0.5 [Kis+08].

It is also possible to focus the electron beam to an atomic-size probe, and use the probe to scan across the sample. The image is formed by measuring the intensity of transmitted or scattered electrons at every scanning position. This imaging mode is called scanning transmission electron microscopy (STEM). One popular technique to detect the intensity of electrons in STEM is high angle annular dark

field (HAADF). As Figure 1.2 shows, an annular detector collects the electrons that are scattered to high collection angles (> 60 mrad). Ideally, the intensity of the electrons scattered to such high angles increases monotonically with respect to the mass and thickness of materials. In comparison, when imaging crystalline materials, TEM images are affected by diffraction of electons in addition to the sample thickness, which makes interpretation difficult [Küb+05].

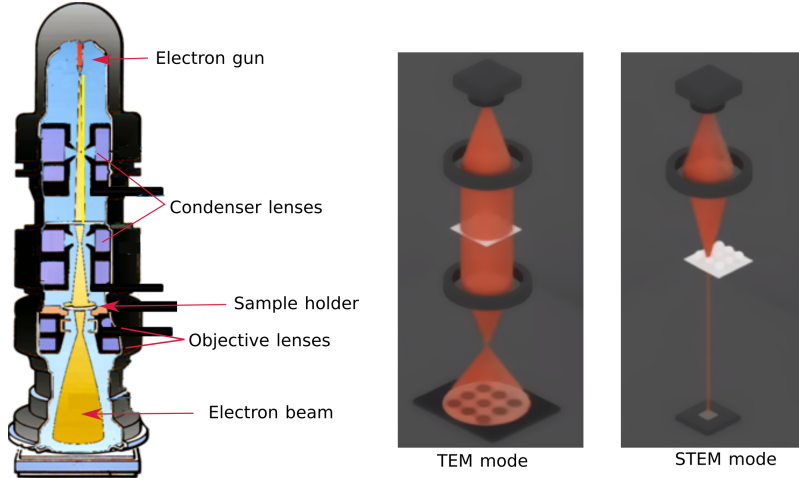

TEM mode   STEM mode

Figure 1.1: Overview of a TEM. Accelerated electrons are generated by the electron gun. In TEM mode, a parallel electron beam is formed by the condenser lenses and used to illuminate the sample placed on the sample holder. The objective lenses form an image of the sample. In STEM mode, the electron beam is focused to a small probe by a set of condenser lenses and an objective lens. The probe is used to scan across the sample. The intensity of transmitted or scattered electrons is measured as the image intensity at each scanning position. (The pictures are adapted from wikipedia.org.)

The monotonic relationship between signal intensities and sample thickness is an important property of HAADF-STEM [Mid+01]. Consider a sample of thickness t with homogeneous attenuation coefficient μ as illustrated in Figure 1.3. Assume that the HAADF detector collects almost all the electrons scattered to angles higher than the inner collection angle of the annular detector, which are complementary to the electrons passing through the hole. According to the Beer-Lambert law, the intensity of electrons that are transmitted or scattered to small angles is approximately given by:

$$I_t = I_0 \exp(-\mu t), \qquad (1.1)$$

where I_0 is the intensity of the incident electron beam. As a result, the complementary HAADF signal intensity I is:

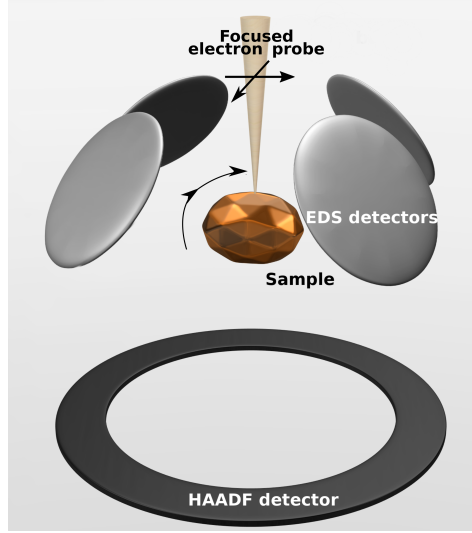$$I = I_0 - I_0 \exp(-\mu t). \qquad (1.2)$$

Figure 1.2: Schematic of simultaneous HAADF and EDS imaging in STEM mode. The focused electron probe moves in directions perpendicular to the beam direction. The HAADF detector collects the electrons scattered to high angles. The four EDS detectors are positioned symmetrically around the sample, and collect the X-rays emitted from the sample. The sample can be tilted by rotating the sample holder (not shown in this figure) for tomographic experiments.
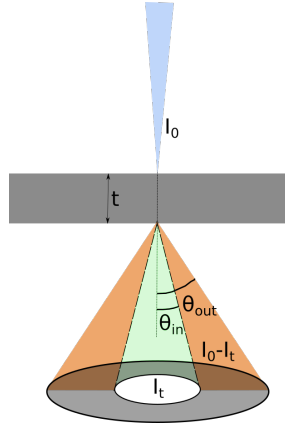

Figure 1.3: Electrons scattered by a thin specimen. The specimen has a thickness of t and a homogeneous density. An incident beam with intensity I_0 is focused on the sample. I_t, which is the intensity of electrons transmitted or scattered to angles smaller than the inner collection angle θ_{in}, can be modeled by the Beer-Lambert law. Assuming that the electrons scattered to angles higher than the outer collection angle θ_{out} are few, the intensity of electrons collected by the detector is given by $I_0 - I_t$.

For small μt, a *linear* approximation of Eq.1.2 can be derived using the Taylor

expansion:

$$I \approx I_0 \mu t, \tag{1.3}$$

which indicates that the signal intensity is approximately linearly proportional to the sample thickness weighted by the attenuation coefficient [MW03]. In practice, the validity of the linearity assumption is affected by a variety of factors, such as the atomic number and thickness of sample, the inner and outer collection angle of the annular detector as well as the accelerating voltage [AR16].
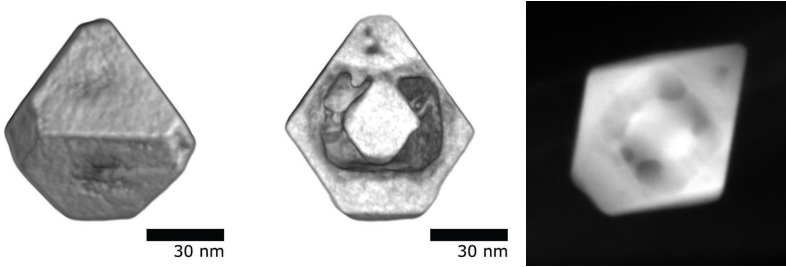

Figure 1.4: HAADF-STEM for a Au-Ag nanoparticle. Left: volume rendering of the tomographic reconstruction of the sample. Middle: inner structure of the reconstruction. Right: a HAADF-STEM projection image for the nanoparticle. (The pictures are adapted from [Zan+16a]. The sample is prepared by the Bionanoplasmonics Laboratory, CIC biomaGUNE, Spain. The HAADF-STEM projection data is provided by EMAT, University of Antwerp, Belgium.)

Another property of HAADF-STEM is that the signal intensity also depends on the atomic number Z of the projected materials, which is referred to as the *Z-contrast*. Based on empirical studies, the attenuation coefficient μ is proportional to Z^α, where α approaches 2 for an ideal detector [Mid+01; Tre11]. The image contrast depending on Z can show the variation of chemical composition and be used for compositional analysis.

However, when the difference in Z is small or chemical elements are mixed, compositional analysis based on HAADF-STEM is difficult. For example, Figure 1.4 shows the HAADF-STEM image of a nanoparticle composed of Au ($Z = 79$) and Ag ($Z = 47$) that are alloyed. It is difficult to separate the Au and Ag in the projection image, while knowing their concentrations is essential for understanding the sample.

In these situations, it is possible to apply spectroscopic techniques that resolve chemical information based on analyzing the energy of radiation (electrons, X-rays, etc.). The spectroscopic techniques that can be combined with STEM include energy dispersive X-ray spectroscopy (EDS) [Gen+12; Lep+13; CM17] and electron energy loss spectroscopy (EELS) [Jar+09; Yed+12; Hab+14]. Both techniques can be used for chemical mapping since the signal intensities are related to the concentrations of chemical elements, and have their own strengths and weaknesses. For example, EDS is more suitable for elements with high atomic numbers compared to EELS, and vice versa. In this thesis we focus on EDS, motivated by the

challenge of imaging semiconductor components in 3D at the nanoscale. In this application domain the key chemical elements match well with the applicability scope of EDS. Moreover, the methods developed in this thesis potentially can be adapted for EELS, as both techniques yield element-specific images.

Figure 1.2 also shows a modern EDS detection system with four energy-resolved X-ray detectors positioned symmetrically around the sample. For each scanning position in STEM mode, the energy-resolved detectors collect the X-rays emitted by the atoms that are excited by the electron beam. The detectors also measure the energy of every incoming X-ray photon, and generate raw data as a three-dimensional (3D) data cube that is illustrated in Figure 1.5. In each pixel of the 2D array of the data cube, there is a spectrum of X-ray counts for over 1000 energy channels. Such a data cube is called a *spectral image.* Figure 1.6 shows examples of EDS spectra for one pixel and for all X-rays integrated over all pixels. From the spectral image, characteristic X-rays, which are emitted from transitions between different electronic shells of a certain chemical element, are integrated over a narrow band of energy channels to form an image. The image can be seen as the 2D projection of the concentration of an element, and is referred to as the *elemental map* [WC16, Chapter 16]. Figure 1.7 shows the elemental maps for Au and Ag of the nanoparticle in Figure 1.4.

While HAADF-STEM gives the projection of all atoms, EDS yields multiple elemental maps, each showing the concentration of a single element. For a thin-film sample with a uniform thickness, assuming that the variation of electron intensity and the interaction between the generated X-rays and the sample are negligible, the image intensity I_a, which is the intensity of characteristic X-rays for element a, is proportional to the sample thickness t and the concentration of the element [WW06]. This relationship is expressed as:

$$I_a = \zeta_a D C_a \rho t, \tag{1.4}$$

where ζ_a is the sensitivity factor, D is the total electron dose, C_a is the concentration of chemical element a, ρ is the density. The mass-thickness of element a is given by $C_a \rho t$.

The sensitivity factor ζ is defined in the so-called ζ-factor method for quantifying the elemental compositions in a sample based on the EDS signal intensity [WW06]. Theoretically, the ζ factor is determined by the ionization cross-section, the fluorescence yield, the relative transition probability, the atomic weight, the detector collection-angle, and the detector efficiency. In practice, the value for a specific element can be estimated using a pure-element standard sample, given that the signal intensity, the total electron dose, and the mass-thickness are known. Quantifying the elemental compositions based on the ζ-factor is a relatively recent development. A more common approach is the so-called Cliff-Lorimer approach, which relates the the signal intensities to the elemental compositions but not to the concentration of a specific element [CL75]. Moreover, the accuracy of this method is limited when lacking calibration samples of which the compositions are accurately known. The accuracy of the ζ-factor method was also limited in the past

due to the difficulty in precisely measuring the thickness of the standard sample.
Zanaga *et al.* propose to estimate the ζ factors based on thickness measured using
electron tomography which makes the ζ-factor method more reliable and feasible
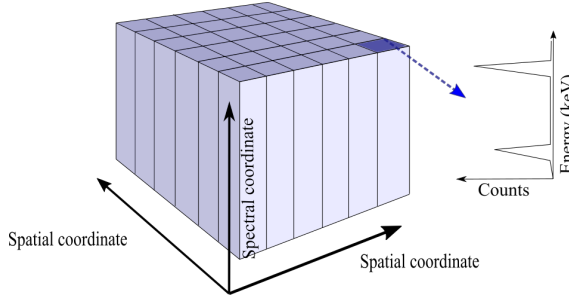[Zan+16b].

Figure 1.5: Schematic of the EDS data cube acquired in STEM mode. The data cube (spectral
image) consists of a full spectrum in each pixel in a 2D array. Each spectrum contains the X-ray
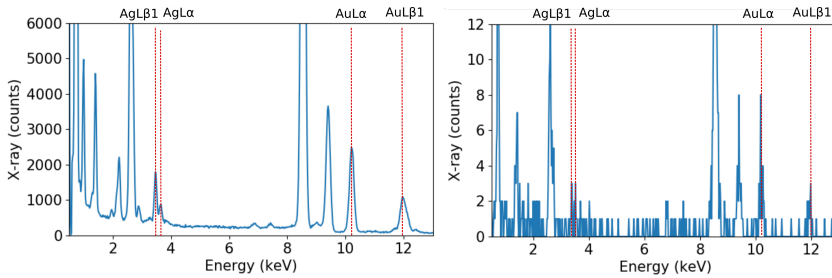intensities at 1000 or more energy channels.

Figure 1.6: EDS X-ray spectra for the Au-Ag nanoparticle showing in Figure 1.4. Left: all
counts integrated over all pixels. Right: X-ray counts of one pixel of the $128 \times 128 \times 1024$ spectral
image. The dashed lines indicate the characteristic energies for Au and Ag. Elemental maps
are extracted by integrating X-ray counts over the energy channels near the characteristic lines.
(The EDS data is provided by EMAT, University of Antwerp.)

The most critical issue for EDS mapping is the strong noise, as the examples
in Figure 1.7 show. The noise is mainly due to the small number of X-ray photons
being detected (e.g. less than 10 counts per pixel) [WC16, Chapter 16]. A key
factor limiting the X-ray detection is the small area covered by detectors. While
the possibilities of X-ray emission in all directions are the same, the maximal
total solid angle covered by the four detectors is about 0.7 sr, which means only
about 6% of the emitted X-rays can be collected [Kra+17] compared to the full
4π emission solid angle. The signal-to-noise ratio can be enhanced by applying a
higher electron dose. This can be realized by increasing the scanning time and/or
the beam current. However, a long scanning time is often accompanied by spatial
drift of the sample, and increasing the beam current is limited by how much current
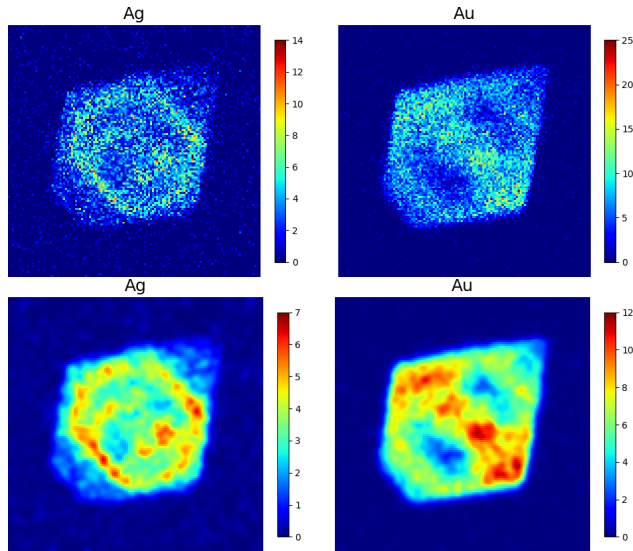
Figure 1.7: EDS elemental maps for Au (right) and Ag (left) of the Au-Ag nanoparticle showing in Figure 1.4, before (upper row) and after (lower row) being smoothed by a Gaussian filter. Note that the X-ray intensities are low (less than 25 counts), and therefore strong Poisson noise is present. (The EDS data is provided by EMAT, University of Antwerp.)

the sample can withstand.

So far, we have discussed acquiring 2D projection images using HAADF-STEM and EDS. In many research domains, such as research on the production of semiconductors, characterizing the 3D structure is crucial for understanding the physical properties. 3D imaging for nanomaterials is often performed by electron tomography (ET) – a technique to reconstruct 3D structures from a series of 2D projection images taken in different directions [SM12], [WC16, Chapter 12]. In an experiment of ET, the sample is placed on a holder which can be tilted to a certain range of angles, as illustrated in Figure 1.2 and Figure 1.8. At a certain tilt angle, a projection/spectral image is acquired using HAADF-STEM/EDS/EELS, after which the sample is rotated, and another image is acquired. At the end of the experiment, one or more tilt series of images are acquired. From a tilt series, a 3D object can be obtained using a reconstruction algorithm. Reconstruction algorithms are based on the assumption that the image intensities are proportional to the integration of some properties of the sample. The assumption is referred to as the *projection requirement*. The projection requirement is satisfied for HAADF-STEM and EDS if the assumptions for the monotonic relationships are valid (Eq.1.3 for HAADF-STEM and Eq.1.4 for EDS).
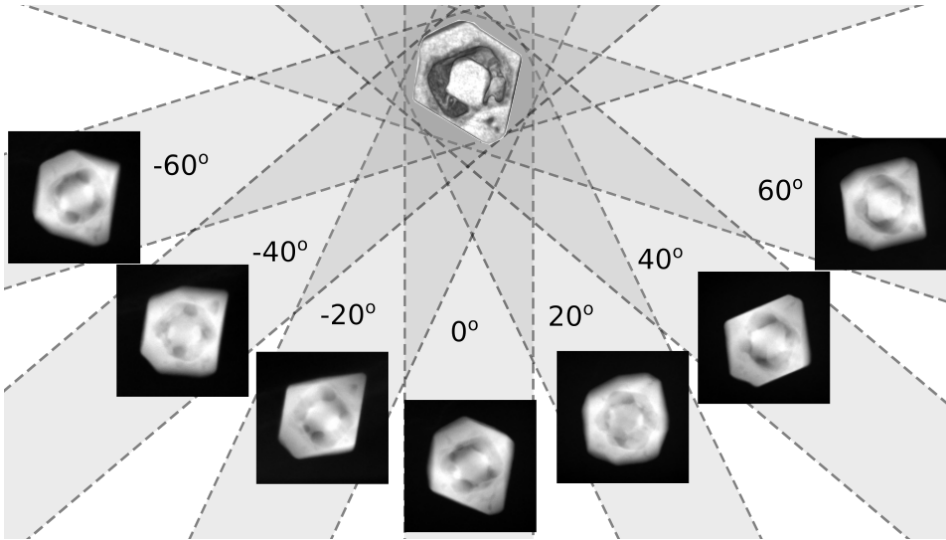
Figure 1.8: A series of HAADF-STEM images for a tomographic experiment in which a sample is tilted over an angular range of $\pm 60°$. For HAADF-STEM tomography, the increment of tilt is usually $1°$ or $2°$

1.2 Mathematics of tomography

In this section, we will introduce the mathematical model for tomographic imaging, which is fundamental for developing novel reconstruction algorithms. Consider an electron probe with a small convergence angle (e.g. 10 mrad) and a large depth of field (e.g. 25 nm). We can approximate the probe as a ray and consider the STEM imaging process as a *parallel beam* tomographic model. When the sample is rotated over a single axis, the data collected for each slice orthogonal to the rotation axis is independent from the other slices. In this case, the 3D parallel beam model can be considered as a stack of 2D parallel beam models. In this section, we will discuss the 2D model.

1.2.1   The Radon transform

The parallel beam model can be mathematically described by the *Radon transform*. The Radon transform for 2D parallel beam is illustrated in Figure 1.9. Consider the object to be reconstructed as a function $f : \mathbb{R}^2 \to \mathbb{R}$. The projection data for the sample tilted by angle θ and the ray at scanning position u is a function $P : [0, \pi] \times \mathbb{R} \to \mathbb{R}$. Radon transform maps f to P as the integral of f along the line $l_{\theta,u}$ described by $u = x \cos \theta + y \sin \theta$, where x and y correspond to the spatial coordinates centered at the rotating axis. The projection $P_\theta(u)$ of $f(x, y)$ is given by:
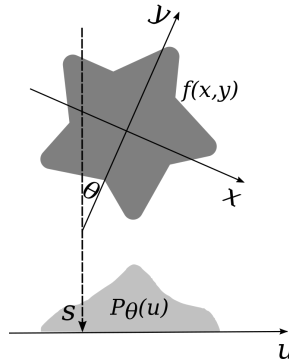
Figure 1.9: Schematic of the Radon transform of function f in 2D. The sample is tilted by angle θ. The ray at scanning position u is described by the line $u = x\cos\theta + y\sin\theta$. The projection data $P_\theta(u)$ of $f(x,y)$ is given by the line integral of $f(x,y)$ along the line.

$$P_\theta(u) = \int_{l_{\theta,u}} f(x,y)\mathrm{d}s, \tag{1.5}$$

where s is the length along line $l_{\theta,u}$.

In practice the data are measured as a discrete sampling of the continuous model, which is illustrated in Figure 1.10. The projection data are expressed as a vector $\mathbf{p} \in \mathbb{R}^M$, where M denotes the total number of pixels for all tilt angles combined. Consider the sample to be located in a 2D space discretized into N pixels as an image. The reconstructed unknowns are then expressed as a vector $\mathbf{x} \in \mathbb{R}^N$, each entry of which corresponds to a pixel value of the 2D image. For each ray i, the projection data p_i is then modeled as the weighted sum of the pixel values x_j along the ray, which is expressed as:

$$p_i = \sum_j^N w_{ij} x_j. \tag{1.6}$$

Each weight w_{ij} is determined by the area of pixel j intersected with ray i. The full set of equations for all rays is:

$$\mathbf{p} = \mathbf{W}\mathbf{x}. \tag{1.7}$$

The multiplication of matrix $\mathbf{W} = \{w_{ij}\}$ and $\mathbf{x}$ is called the *forward projection* of $\mathbf{x}$. The goal of tomographic reconstruction is to estimate the unknowns $\mathbf{x}$ from the data $\mathbf{p}$.

1.2.2 Reconstruction algorithms

One group of reconstruction algorithms is based on inverting the Radon transform Eq.1.5 to find an analytical expression for $f(x,y)$, which is known as the analytical
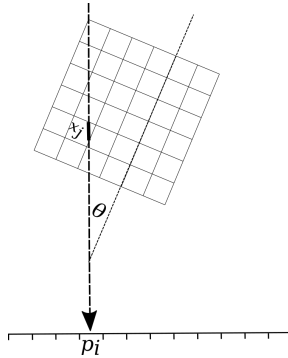
Figure 1.10: Schematic of the discrete linear projection model in 2D. The unknown corresponding to pixel j is denoted by x_j. The measurement data corresponding to the i_{th} ray is denoted by p_i. The contribution of x_j to p_i is given by $w_{ij}x_j$, where w_{ij} is determined by the area of pixel j intersected with ray i (indicated in bold).

reconstruction methods. A widely used analytical reconstruction method is *filtered backprojection* (FBP) [KS88, Chapter 3]. The FBP method has the advantage of being computationally efficient, as it only consists of a convolution operation and an integration operation. However, the analytical methods are based on the assumption that there is an infinite number of projections available. When only a limited number of projections are acquired, artifacts will appear in the reconstruction. Another group of reconstruction methods which are based on inverting the discrete model Eq.1.7 is called algebraic reconstruction methods. These methods tend to handle the problem of limited number of projections better than the analytical methods, as they do not assume that infinite number of projections are available. The unknown $\mathbf{x}$ is usually determined such that if we compute the projection of it, the *data discrepancy* $\mathfrak{D}(\mathbf{Wx}, \mathbf{p})$ between the measured $\mathbf{p}$ and the reprojected data $\mathbf{Wx}$ is minimized, which is expressed as:

$$\mathbf{x}^* = \underset{\mathbf{x}}{\operatorname{argmin}}\, \mathfrak{D}(\mathbf{Wx}, \mathbf{p}). \qquad (1.8)$$

The data discrepancy is often defined as the squared l_2 norm of the difference between $\mathbf{p}$ and $\mathbf{Wx}$: $\| \mathbf{Wx} - \mathbf{p} \|_2^2$. The minimization problem can be solved by iterative algorithms, such as algebraic reconstruction technique (ART) [GBH70] and simultaneous iterative reconstruction technique (SIRT) [GB08]. Compared to the analytical algorithms, the algebraic algorithms result in fewer artifacts when data are missing or noisy. Over-fitting to noise can be prevented by stopping the algorithm early (e.g. at tens of iterations), however, at the cost of not being able to reconstruct fine structures [ENH10].

In addition to the quadratic functional, non-quadratic functionals such as Student's t, Kullback–Leibler divergence and negative log-likelihood have been examined extensively for tomographic reconstruction considering the statistical properties of the measurement data. In particular, the Kullback–Leibler divergence and

the negative log-likelihood are often used for data that are Poisson noise limited [HW16; ER07], while the quadratic functional is based on Gaussian noise model. Minimizing the data discrepancy often converges to the same result as maximizing the likelihood for measuring the data. Examples of the latter approach are the maximum likelihood estimation (MLE) and the maximum a posteriori (MAP) estimation [SV82; Gre90], which are often applied on emission tomography assuming that the measured data are random variables obeying certain statistical models.

To yield more accurate reconstructions, a popular approach is to incorporate prior knowledge about the reconstructed object [BO13; Bat+09]. The prior knowledge is often implemented as a regularization term added to the minimization problem:

$$\mathbf{x}^* = \underset{\mathbf{x}}{\operatorname{argmin}} \, \mathfrak{D}(\mathbf{Wx}, \mathbf{p}) + \lambda \mathfrak{R}(\mathbf{x}). \tag{1.9}$$

The regularization term $\mathfrak{R}(\mathbf{x})$ is a functional promoting some properties of the reconstructed image, and λ indicates the weight of the regularization term. A well-known example is the total variation (TV) regularization [BO13]. The reconstructed image with penalized TV tends to possess piecewise constant features.

1.3 Challenges and overview

After introducing the mathematics of tomography, we now look at the actual tomographic experiment based on simultaneously acquired HAADF-STEM and EDS. Both imaging modalities have their own advantages and disadvantages. The noise in EDS mapping is a critical issue for computing accurate tomographic reconstructions, as real measurement data deviate from the ideal projection data defined in Eq.1.7. In many EDS tomographic experiments, the noise issue is addressed by image filtering before and after reconstruction at the cost of reducing resolution [Zan+16a; Sla+16a]. The noise can also be reduced using multivariate statistical analysis methods which separate the noise from the spectral image, but with limited effectiveness when the noise dominates the data [Bur+16; Jol02].

Moreover, the number of tilts in EDS tomography is usually limited (e.g. 29 tilts for $\pm 70°$), as it takes a long time to acquire enough X-rays in every scan (about 5 to 10 mins). Consequently, it is difficult to reconstruct accurately with information from many angles missing. Furthermore, the projection matrix $\mathbf{W}$ is often ill-conditioned. This means that even small noise in measurement data can cause large errors in the reconstruction. The strong noise, together with the limited number of tilts and the ill-conditioned matrix, poses strong challenges for EDS tomographic reconstruction. Other challenges in EDS tomography include detector shadowing [Sla+16b; Sla+16a] as well as X-ray absorption and fluorescence [WW06]. The sample holder causes shadowing of X-rays on the detector, and consequently the signal intensity varies as a function of the tilt angles. To addressed the influence on the reliability of the tomographic reconstruction, novel correction methods have been proposed, such as adjusting the acquisition time at different tilts based on the detector geometry [Kra+17] and compensating the

angle-dependency in combination with HAADF-STEM tomography [Zan+16a]. In addition, an X-ray absorption correction method for EDS tomography has been proposed [Bur+16], showing improved reconstruction results. Although these effects are not the focus of this thesis, they should be carefully considered especially when conducting quantitative EDS tomography.

Compared to EDS, HAADF-STEM can yield a larger number of tilt images (e.g. 141 tilts for $\pm 70°$) with much higher signal-to-noise ratios, and consequently can lead to reconstructions with less noise and higher resolution. In addition, variation of chemical elements can be characterized based on the HAADF reconstruction as long as the difference in contrast is mainly contributed by the difference in Z. Thus, it is possible to obtain element-specific 3D objects by segmenting the HAADF-STEM tomographic reconstruction based on the Z contrast. However, this is only applicable to samples of segmentable compositions with large difference in Z.

Table 1.1 compares some properties of HAADF-STEM and EDS tomography in terms of the chemical information, noise, and the number of tilts. These properties of the two simultaneously performed modalities are complementary to each other. Attempts have been made to combine HAADF-STEM tomography and EDS tomography. For instance, HAADF-STEM tomography has been combined with EDS tomography for projection alignment, joint analysis and thickness estimation [Gor+14; Bur+16; Kra+17]. In particular, an approach has been proposed to combine HAADF-STEM and EDS tomography to acquire quantified element-specific reconstructions [Zan+16a]. In this approach, the HAADF-STEM reconstruction is computed to estimate the sample thickness which is then combined with the ratio maps of elements obtained by EDS. Given these promising results, **the overarching goal of this thesis is to explore novel methods that combine HAADF-STEM and EDS tomography to acquire accurate and element-specific reconstructions.**

Table 1.1: HAADF-STEM tomography vs EDS tomography

	HAADF-STEM	EDS
Chemical information	mixed	element-specific
Noise level	low	high
Number of tilts	large	small

As it turns out, to successfully combine the strengths of HAADF-STEM and EDS tomography, many challenges must be solved, including developing novel algorithms that can combine both modalities, making these advanced approaches generally applicable, as well as solid modeling of the image formation. This thesis mainly addresses four challenges as follows.

First, knowing that EDS maps each chemical element and HAADF-STEM maps all elements combined, one can combine the two modalities in one reconstruction process.The simultaneous reconstruction process needs to be based on a

tomographic model that is consistent with both modalities.

In Chapter 2, we introduce a technique to reconstruct for all elements simultaneously from EDS elemental maps and HAADF-STEM projection images, which is named HAADF-EDS bimodal tomography (HEBT). We assume that the HAADF-STEM projection images are the weighted sum of EDS maps for all present chemical elements. We therefore introduce a linear sum constraint to a reconstruction process for all elements, which can be solved using an iterative algorithm.

Second, while HEBT requires EDS mapping for all the chemical elements imaged by HAADF-STEM, which may be impossible sometimes, we need a different combining strategy which can be applied to one element each time. A clear combining strategy is to encourage the Z-contrast reconstruction and the element-specific reconstruction to preserve consistent image features such as common edges. The remaining questions include what feature to exploit and how to incorporate the consistency in the reconstruction process.

In Chapter 3, HAADF-STEM and EDS is combined in a way different to HEBT. We penalize so-called total nuclear variation (TNV) of a Z-contrast reconstruction made from HAADF-STEM data and an element-specific reconstruction made from EDS data, to encourage common edge locations and parallel/antiparallel gradients. This combining approach can be applied to the reconstruction for one element each time.

Third, in addition to combining modalities, many advanced reconstruction methods can also be applied to improve the accuracy of reconstruction. However, these methods are based on different assumptions for the sample and the imaging process, and a clear guideline for deciding which algorithms to use is still missing in the field of HAADF-STEM + EDS tomography. It is also possible to combine algorithms with different strengths and weaknesses in one reconstruction framework to obtain optimal results. Therefore, a framework for applying the algorithms needs to be developed.

In Chapter 4, we propose the framework to combine different advanced reconstruction algorithms for HAADF-STEM + EDS tomography. Algorithmic recipes composed of different ingredients can be applied to augment tomographic reconstruction. The ingredients mainly belong to three modules: statistical modeling, variational regularization, and HEBT. To incorporate the correct prior knowledge and physical constraints, we also provide guidelines to tailor recipes based on the experimental conditions and the samples.

Finally, the linear integral model is fundamental for combined tomographic reconstruction. However, the linearity assumption can be invalid for thick samples. For EDS, the nonlinear signals are mainly caused by the X-ray absorption of the sample. For HAADF-STEM, when the sample is thick, the signal intensity damps at large thickness as illustrated in Eq.1.2. While numerical methods to correct the absorption in EDS tomography have been proposed [Bur+16], numerical methods that require no extra experimental step to correct the intensity damping in HAADF-STEM tomography are missing.

To address the nonlinear damping effects in HAADF-STEM data, we propose an automatic correction algorithm for samples consisting of homogeneous compo-

sitions, which is described in Chapter 5. The correction algorithm only requires the projection images as input. A nonlinear model is estimated based on the reconstructed structure as well as the errors between linearly re-projected data and measurement data. It is possible to use the correction algorithm together with the correction for X-ray absorption to improve the accuracy of HAADF-STEM + EDS tomography.